Research Square

Preprints are preliminary reports that have not undergone peer review.
They should not be considered conclusive, used to inform clinical practice,
or referenced by the media as validated information.

Modular Adaptive Strategies for the Leaf Anatomical Traits of Phoebe zhennan across Karst Regions

EnYi Dai
Guizhou University
Hong Luo
luohong841014@sina.com
Guizhou Academy of Forestry
HengFeng Jia
Guizhou Academy of Forestry
ShaSha Wang
Guizhou Academy of Forestry
YunLi Jiang
Guizhou Academy of Forestry
YanBing Yang
Guizhou Academy of Forestry
FengXia Yan
Guizhou Academy of Forestry

Research Article

Keywords: Phoebe zhennan, leaf anatomical traits, karst regions, modular adaptation, spatial autocorrelation

Posted Date: November 23rd, 2026

DOI: https://doi.org/10.21203/rs.3.rs-11646227/v1

License: This work is licensed under a Creative Commons Attribution 4.0 International License.
Read Full License

Additional Declarations: No competing interests reported.

Abstract

Background

Karst regions are highly heterogeneous, where leaf anatomical trait adaptation is key for plants to cope with multiple stresses. However, the adaptive strategies of *P. zhennan*, a vulnerable endemic tree species, remain poorly understood. This study aimed to elucidate its leaf anatomical adaptations across karst regions.

Results

Among the 16 measured traits, eight core traits were identified and grouped into three functional modules. The three predictor groups collectively explained 44.8% of the total variation, with soil factors having the highest independent explanatory power (20.3%), followed by spatial (18.2%) and climatic factors (13.6%). Trait variation was governed predominantly by independent main effects, whereas interactive effects were negligible. The three functional modules exhibited distinct adaptive strategies driven by different dominant factors: the protective module presented high plasticity with nonlinear responses to climatic and soil factors; the conductive module presented a safety–efficiency trade-off that was shaped mainly by soil and spatial factors; and the photosynthetic module maintained coordinated adjustments between palisade and spongy tissues to optimize light capture, which was predominantly regulated by spatial factors, with secondary contributions from climate and soil.

Conclusions

This study demonstrated the modular organization of leaf anatomical traits in the karst tree *P. zhennan* and quantified the differential effects of soil, spatial, and climatic factors on distinct functional modules. These findings not only reveal the modular adaptation strategies of this species in heterogeneous habitats and provide functional trait-based criteria for prioritizing germplasm conservation in natural populations but also extend the application of modular analysis from temperate or model species to adaptive studies of karst forest trees.

1 Introduction

As the primary interface between plants and the atmosphere, leaves integrate photosynthesis, transpiration, and defense [1], with their morphology reflecting long-term adaptations to abiotic constraints [2]. The leaf economics spectrum (LES) posits a fundamental trade-off between resource acquisition (e.g., high photosynthetic rates) and conservation (e.g., leaf lifespan) [3], driving divergent adaptive strategies across latitudinal gradients [4]. Leaf traits typically exhibit predictable plasticity along gradients of water, nutrient, and light availability. For example, shade-adapted species often maximize light capture by increasing the specific leaf area (SLA) [5], whereas high-light environments favor

investments in structural defenses, such as increased leaf mass per area (LMA) [6]. However, these macroscale adjustments in leaf morphology are ultimately underpinned by modifications in leaf anatomical architecture [7].

Leaf anatomical architecture—comprising protective tissues, mesophyll, and vascular systems—exhibits remarkable plasticity, which underpins intraspecific variation in morphology and mediates key physiological processes [7–9]. Specifically, mesophyll configuration and leaf thickness critically regulate carbon assimilation and water loss [10, 11], whereas the architecture of vascular networks governs hydraulic transport, mechanical support, and carbon allocation strategies [12]. For example, plants have been shown to adapt to rising temperatures and precipitation by expanding the proportional thickness of palisade tissue and shrinking the fraction of spongy mesophyll [13]. In addition, under low-light or saline conditions, plants frequently reduce their epidermal and leaf thicknesses to minimize CO_2 diffusion limitations [14, 15]. This anatomical plasticity represents a fundamental mechanism enabling plant persistence in heterogeneous habitats [16, 17].

Traits do not vary in isolation; traits that share developmental pathways or serve a common function tend to covary, so phenotypes are organized into integrated functional units rather than independent traits [18]. Correlation networks derived from multitrait datasets typically yield functionally interpretable clusters rather than a single global variation axis [19, 20]. Modularity arises whenever functional specialization, shared ontogeny and pleiotropy concentrate covariance within a group of traits, whereas functional differentiation and even conflicting selection pressures limit covariance across sets of traits [21, 22]. In plants, this line of thinking has developed into the distinct concept of “modular phenotypic plasticity” [23, 24]. Therefore, modularity is not merely a statistical description of the trait matrix; it is an organizational property that enables plants to regulate different functions semiindependently without losing the functional integrity of the whole [25]. However, although leaf modularity has been demonstrated within a single species, most of this evidence is based on whole-plant trait networks involving morphological and economic traits [26, 27]. It remains largely untested whether modules can be identified from anatomical traits within a single species and whether their modular structure is stable across geographically isolated populations. Given that the relationship between integration and plasticity itself remains controversial, this gap is particularly striking [28, 29]. Drivers of trait variation are typically examined category by category, but climate, soil, and spatial predictors are rarely decomposed simultaneously within the same dataset [26, 30, 31]. Therefore, it is impossible to determine whether different modules are indeed driven by different selection factors. The relationship between traits and the environment is almost always modeled as monotonic, even though the costs and benefits of leaf investment should vary discontinuously along a resource gradient; when the response is nonlinear, a linear model captures only a segment of the curve [32].

P. zhennan is a tree species endemic to China’s subtropical regions. It is widely distributed in areas below 1,500 m in elevation and has attracted significant attention because of its economic value and ecological functions [33]. However, the natural range of *P. zhennan* populations is becoming increasingly restricted, natural resources are on the verge of depletion, and their genetic diversity is under threat [34].

It is listed as a threatened species by the International Union for Conservation of Nature (IUCN) [35]. In response to heterogeneous environments, *P. zhennan* exhibits pronounced plasticity across phenotypic, anatomical, and physiological traits. Previous studies have indicated that drought stress induces elevated antioxidant enzyme activity (e.g., SOD and POD) and osmotic adjustments via proline accumulation [35, 36], alongside the development of a thicker cuticle to mitigate radiation damage and water loss [37]. Additionally, *P. zhennan* enhances light capture in low-light environments by increasing leaf area [38] and improves frost tolerance through the synthesis of soluble sugars [39]. The karst region in southwestern China is an important distribution area for *P. zhennan* and contains the largest natural resources of this species in China [40, 41]. The extensive karst topography generates profound spatial heterogeneity in hydrothermal conditions and soil properties, creating a diverse array of small-scale habitats [42, 43]. This heterogeneity provides an ideal setting for studying the modular adaptation of leaf anatomical traits. Therefore, this study examined 25 native populations of *P. zhennan* in the karst regions of southwestern China and measured 16 anatomical traits, aiming to systematically analyze how their leaf anatomical traits respond to climatic, soil, and spatial factors. On the basis of these findings, we propose the following core hypothesis: the anatomical traits of *P. zhennan* leaves exhibit modularity; different modules can respond relatively independently to their respective primary environmental selection pressures (i.e., climate conditions, soil properties, and spatial heterogeneity), thereby forming a modular adaptive strategy; and some of these responses may follow a nonlinear pattern. This study aims to test the above hypotheses, confirm the existence of a modular anatomical structure in the leaves of *P. zhennan*, and elucidate how modular adaptation operates in this species within heterogeneous karst habitats, thereby providing a theoretical basis for the conservation of this rare tree species and the restoration of karst ecosystems.

2 Materials and methods

2.1 Study area

This study was conducted across nine counties/districts within the karst region of southwestern China, including Bozhou, Chishui, Dejiang, Huishui, Jinsha, Sinan, Shiqian, Wuchuan, and Xishui. These sites collectively encompass 25 representative natural populations of *P. zhennan* (Fig. 1). The study area spans 105.68°–108.84° E and 25.86°–28.90° N, with elevations ranging from 208 to 1,212 m. The regional climate is characterized by a subtropical humid monsoon, with mean annual temperatures (MAT) ranging from 15.1 to 17.2°C and mean annual precipitation (MAP) ranging from 1,050–1,350 mm.

2.2 Sample collection

The samples were collected from natural populations between November and December 2024. In each population, 3–10 healthy, mature *P. zhennan* trees were randomly selected. From the sun-exposed side of the middle canopy of each tree, five fully expanded, pest-free leaves were collected, numbered, immediately placed in 70% FAA fixative for fixation, and then transported to the laboratory. The collection of plant samples complied with institutional, national, and international guidelines, and was authorized

under the provincial forest germplasm resource collection plan. The plant samples used in this study were identified by Yan-Bing Yang, a plant taxonomist, primarily through cross-comparison with voucher specimens deposited at the Herbarium of Guizhou Academy of Forestry. No new voucher specimens were prepared for this study.

2.3 Leaf anatomical trait measurement

The collected leaf segments were fixed, dehydrated through a graded ethanol series, cleared, embedded in paraffin, and sectioned at 12 μm using a rotary microtome (RM2235, Leica Inc., Bensheim, Germany). The sections were affixed to slides, dried, deparaffinized, stained with safranin-O and fast green, and mounted with coverslips. Observations and photographs were taken using a light microscope (Olympus BX53 (LED), Japan). ImageJ software (NIH, Bethesda, MD, USA) was used to measure upper cuticle thickness (UCT, μm), upper epidermis thickness (UET, μm), lower epidermis thickness (LET, μm), palisade tissue thickness (PT, μm), spongy tissue thickness (ST, μm), leaf thickness (LT, μm), main vein vascular bundle width (MVBW, μm), main vein vascular bundle thickness (MVBT, μm), main vein xylem thickness (MVXT, μm), upper phloem fiber thickness in the main vein (UPFT, μm), and lower phloem fiber thickness in the main vein (LPFT, μm). The primary vein density (PVD, veins mm^{-1}), main vein diameter–thickness ratio (MD/MT), palisade–sponge ratio (PT/ST), tightness of the leaf tissue structure (LTT), and looseness of the leaf tissue structure (LTL) were calculated. Three measurements were recorded for each section, and the averages were used for subsequent analysis.

(1) Tightness of the leaf tissue structure (LTT) = palisade tissue thickness (PT)/leaf thickness (LT)

(2) Primary vein density (PVD) = number of primary veins intersected/leaf width (measured perpendicular to the midrib)

(3) Looseness of the leaf tissue structure (LTL) = spongy tissue thickness (ST)/leaf thickness (LT)

2.4 Environmental and spatial variables

2.4.1 Climate data

Climatic data were extracted from the China Surface Climate Standard Normals Dataset via the China Meteorological Data Network[44]. Thirty-year (1991–2020) climatological normals of 72 meteorological stations across the study area were collected, including mean annual precipitation (MAP, mm), mean annual temperature (MAT, °C), ≥ 0°C accumulated temperature (≥ 0°C AT, °C·d), ≥ 10°C accumulated temperature (≥ 10°C AT, °C·d), and relative humidity (RH, %). Spatial interpolation was implemented via ordinary kriging within ArcGIS 10.8 (Geostatistical Analyst module) via a spherical semivariogram model. Climatic attribute values corresponding to each *P. zhennan* population were extracted from the generated raster layers and integrated into a tabulated dataset for subsequent analyses.

2.4.2 Soil data

Soil datasets covering total organic carbon (TOC, %), sand content (SC, %), clay content (CC, %), cation exchange capacity (CEC, cmol kg^{-1}), and total nitrogen (TN, g kg^{-1}) were retrieved from the Harmonized World Soil Database version 2.0 (HWSD v2.0)[45]. The targeted soil attribute data were extracted via ArcGIS 10.8 and compiled into a spreadsheet for subsequent analyses.

2.4.3 Spatial variables

The true elevation (Elev, m) of each population was obtained via RTK positioning and served as a variable characterizing the topographic gradient. To quantify residual spatial autocorrelation not explained by elevation or environmental factors, spatial variables were generated via principal coordinates of neighborhood matrices (PCNM) [46, 47]. Pairwise Euclidean distances were calculated on the basis of the projected coordinates of the populations. The truncation threshold was set to the length of the longest edge in the minimum spanning tree (145 km), covering the maximum connectivity distance among all populations within the study area. Following the generation of candidate PCNM axes, forward selection was performed using leaf anatomical traits as the response variable on the basis of permutation tests (α = 0.05); only the significant PCNM axis (PCNM5) was retained. Elev and the selected significant PCNM axes were ultimately incorporated as spatial factors in all subsequent analyses. All spatial analyses were performed in R (v4.6.0) via the 'vegan' and 'adespatial' packages.

2.5 Statistical analyses

Data organization and descriptive statistics were performed in Microsoft Excel, whereas subsequent statistical analyses and visualizations were conducted in R (v4.6.0). To mitigate multicollinearity, variance inflation factors (VIF) were calculated for all candidate climatic, soil, and spatial variables; variables with VIF ≥ 10 were excluded [48]. Ultimately, one climatic variable (MAP), two soil variables (CEC, SC), and two spatial variables (PCNM5, Elev) were retained. A total of 16 leaf anatomical traits were initially measured (see Additional file 1). Using variation partitioning analysis (VPA) and setting a threshold of > 30% for the total explanatory power of each trait, 8 core traits were selected. On the basis of their physiological functions [10–12], these traits are categorized into three functional modules (protective module: UET and LET ;conductive module: MVBW, PVD and LPFT; photosynthetic module: ST, LTT and PT/ST), and the stability of each module is assessed via the covariance ratio (CR) [49]. Normality and homogeneity of variance were assessed via the Shapiro–Wilk test and Levene's test, respectively. On the basis of the test results, the nonparametric Kruskal–Wallis H test (Benjamini–Hochberg correction, α = 0.05) was adopted to compare differences among different *P. zhennan* populations. The phenotypic differentiation coefficient (PST) was calculated to quantify interpopulation divergence in leaf anatomical traits via the following formula: PST $=\sigma_{\mathrm{B}}^2/(\sigma_{\mathrm{B}}^2+\sigma_{\mathrm{W}}^2)$, where σ_{B}^2 and σ_{W}^2 represent the between-population and within-population variance components, respectively, estimated via a linear mixed model (LMM). The relative contributions of environmental and spatial factors to trait variation were quantified via redundancy analysis (RDA) and variation partitioning analysis. To explore nonlinear responses, generalized additive models (GAM) were fitted via the mgcv package. The basis dimension was restricted to k = 4 to prevent overfitting, and select = TRUE was applied to enable automatic smoothing parameter selection via shrinkage penalties; smoothing parameters were

estimated via restricted maximum likelihood (REML). To verify the necessity of nonlinear fitting, linear models (LM) and generalized additive models (GAM) were fitted separately for each trait, and their performance was compared via the Akaike information criterion (AIC). ΔAIC was defined as AIC(LM) − AIC(GAM). The interpretation of ΔAIC follows that of Symonds and Moussalli [50]: When ΔAIC < 2, the two models provide similar support; when ΔAIC > 6, the inferior model can be rejected. The effective spatial scale of PCNM5 was determined via Moran's I autocorrelation diagnostics (grouped into 30-km intervals), and P values at each distance scale were corrected via the Benjamini—Hochberg method (α = 0.05). A partial Mantel test (controlling for MAP, CEC, SC, and Elev) was then conducted to verify whether the spatial structure of PCNM5 was independent of the measured environmental variables.

3 Results

3.1 Modular structure of leaf anatomical traits

The covariance ratio (CR) permutation test confirmed a significant modular structure among the three predefined functional modules (protection, conduction, and photosynthesis; Table 1). The observed CR value was 0.5787, which is substantially lower than the average CR value under random permutation (1.9409) and falls below the lower bound of the 95% confidence interval of the permutation distribution (0.7013). A one-sided left-tailed permutation test indicated that the observed CR was significantly smaller than the expected value under random permutation (left-tailed $P = 0.0089$), suggesting that the eight leaf anatomical traits exhibited statistically significant modularity under the three predefined modules.

Table 1
Results of the covariance ratio permutation test for modularity of leaf anatomical traits

Parameter	Value
Observed covariance ratio (CR)	0.5787
Mean CR under null hypothesis	1.9409
Median CR under null hypothesis	1.6759
95% confidence interval of null CR	[0.7013, 5.6123]
Left-tail P (H_0: no modularity)	0.0089

3.2 Variation in and differentiation of leaf anatomical traits

An analysis of eight leaf anatomical traits across 25 *P. zhennan* populations revealed marked differences in the magnitude of trait variation (Table 2). The coefficients of variation (CV) ranged from 0.152 to 0.307; UET (CV = 0.307) presented the highest variability, whereas LTT (CV = 0.152) presented the lowest variability. All traits except PT/ST and ST differed significantly among populations ($P < 0.05$). The phenotypic differentiation coefficient (PST) varied markedly among the traits (Fig. 2). Protective traits

(UET: 0.45; LET: 0.28) and conductive traits (PVD: 0.51; LPFT: 0.39) presented relatively high values, indicating strong interpopulation differentiation. In contrast, other conductive traits (MVBW: 0.17) and photosynthetic traits (LTT: 0.19; ST: 0.10; PT/ST: 0.05) presented relatively low PST values, indicating weak interpopulation differentiation. Notably, ST and PT/ST presented the lowest PST values across all traits.

Table 2
Variation and differential analysis of leaf anatomical traits in *P. zhennan*.

Functional module	Trait	Maximum value (Site)	Mean (± SD)	Minimum value (Site)	CV	*P*
Protective module	UET	10.96 (SQ1)	6.38 ± 1.96	2.44 (SN2)	0.307	< 0.001***
	LET	14.47 (HS2)	7.65 ± 2.24	2.92 (WC4)	0.292	< 0.001***
Conductive module	LPFT	87.95 (SN5)	48.06 ± 13.45	20.75 (SQ1)	0.280	0.002**
	PVD	276.35 (SQ1)	126.95 ± 37.87	79.48 (DJ3)	0.298	< 0.001***
	MVBW	794.31 (DJ6)	509.89 ± 93.68	206.03 (WC4)	0.184	0.005**
Photosynthetic module	PT/ST	5.26 (JS)	2.2 ± 0.63	1.11 (DJ7)	0.287	0.054
	LTT	0.67 (JS)	0.51 ± 0.08	0.21 (WC4)	0.152	0.017*
	ST	60.57 (WC1)	34.47 ± 9.06	17.19 (CS3)	0.263	0.108

The CV represents the coefficient of variation calculated from pooled data across all populations, reflecting overall trait variability. P values were adjusted via the Benjamini–Hochberg false discovery rate (FDR) procedure to indicate the significance of interpopulation differences: *$P < 0.05$, **$P < 0.01$, ***$P < 0.001$. Abbreviations: UET, pper epidermal thickness (μm); LET, lower epidermal thickness (μm); MVBW, main vein vascular bundle width (μm); LPFT, lower phloem fiber thickness in the main vein (μm); PVD, primary vein density (veins mm^{-1}); ST, spongy tissue thickness (μm); LTT, tightness of the leaf tissue structure; PT/ST, palisade–sponge ratio.

3.3 Relative contributions of environmental and spatial factors

The RDA (Fig. 3b) revealed that the three groups of predictors—climate, soil, and spatial factors—jointly explained 44.8% of the total variation in the leaf anatomical traits. Soil factors independently explained 20.3% of the total variance, followed by spatial factors (18.2%) and climate factors (13.6%). The relative

contributions of individual predictors to the constrained variation were further quantified (Fig. 3c): PCNM5 contributed the most (23.9%), followed by MAP (21.8%), CEC (20.3%), and SC (17.6%), whereas Elev contributed the least (16.5%). The RDA ordination biplot (Fig. 3a) revealed that the first two axes collectively explained 77.15% of the total constrained variation. Axis 1 explained 45.36% of the constrained variation and was associated primarily with PCNM5, Elev, CEC, and MAP; these variables strongly correlated with the variations in PVD, MVBW, ST, PT/ST, and UET. Axis 2 accounted for 31.79% of the constrained variation and was driven mainly by MAP and SC, which were correlated with variations in LET, LTT, and LPFT.

Variance partitioning for individual traits further quantified the independent and joint effects of climatic, soil, and spatial factors (Fig. 4). Traits within different functional modules exhibited distinct differences in their responses to these driving factors. The total variance explained by all factors ranged from 33.9% to 76.4%. Notably, trait variation was predominantly explained by independent effects, whereas joint effects were minimal, ranging from 0% to 9.9%. Within the protective module, LET presented the lowest cumulative explanatory power (33.9%), driven primarily by soil (16.0%) and climate factors (17.9%). UET had a relatively high cumulative explanatory power (48.6%), which was also attributable mainly to soil (15.1%) and climate factors (33.4%). In the conductive module, LPFT, MVBW, and PVD were regulated primarily by soil and spatial factors, with cumulative explanatory powers of 65.3%, 39.4%, and 38.7%, respectively. However, their dominant driving factors differed: LPFT (27.8%) and MVBW (28.8%) were mainly governed by soil factors, whereas PVD was jointly controlled by soil (17.9%) and spatial factors (20.8%), with nearly equal contributions from the two drivers. Within the photosynthetic module, LTT presented the highest cumulative explanatory power (76.4%), which was primarily regulated by soil (30.4%) and spatial factors (23.9%). In contrast, ST and PT/ST had relatively lower cumulative explanatory power (44.9% and 37.1%, respectively), driven predominantly by spatial (38.8%) and climatic factors (19.8%). Additionally, spatial factors had a notable influence on the variation in PT/ST (14.4%).

3.4 Nonlinear responses of leaf anatomical traits to environmental and spatial drivers

Generalized additive models (GAM) revealed the divergent effects of climatic, soil, and spatial drivers on leaf anatomical traits (Fig. 5). The responses varied substantially across functional modules. Model comparisons revealed that the GAM outperform or perform as well as the corresponding linear models (LM) for most traits (see Additional file 2). Within the protective module, the GAM for UET and LET were significantly better than the LM were (ΔAIC values of 5.62 and 10.36, respectively); both UET and LET exhibited nonlinear increasing trends with increasing MAP, and no clear trend was observed below 1,150 mm, followed by a steeper increase above this threshold (Fig. 5a, b). LET also exhibited nonlinear responses to CEC, with an initial increasing trend followed by stabilization (Fig. 5c), and displayed a U-shaped response to PCNM5 (Fig. 5e). Additionally, LET increased linearly with SC (Fig. 5d). In the conductive module, the GAM for MVBW are slightly better than the LM (ΔAIC = 2.13); MVBW shows a nonlinear response to PCNM5, which initially increases and then plateaus (Fig. 5j) but decreases linearly

with the CEC and SC (Fig. 5h, i). For the remaining conductivity traits, there was little difference between the GAM and LM (ΔAIC < 2), and both showed linear responses in the figure: the LPFT increased linearly with MAP and SC (Fig. 5f, g), whereas the PVD decreased linearly with the CEC (Fig. 5k). In contrast, although the GAM for PT/ST in the photosynthetic module performed slightly better than those for LM (ΔAIC = 2.40) and the differences between the GAM and LM for ST and LTT were both small (ΔAIC < 2), all the traits exhibited linear relationships with environmental and spatial factors. Specifically, ST increased linearly with PCNM5 (Fig. 5l), LTT rose linearly with SC and Elev (Fig. 5o, p), and PT/ST increased with MAP (Fig. 5m) but declined with PCNM5 (Fig. 5n).

3.5 Validation of the spatial structure of PCNM5 via Moran's I

To verify whether PCNM5 effectively captured the inherent spatial structure, Moran's I autocorrelation analysis was performed with distance classes defined at 30 km intervals (Table 3). The results indicated that PCNM5 showed complex spatial autocorrelation along the distance gradient, with significant positive autocorrelation at a midpoint distance of 17.9 km (I = 0.452, *P* = 0.006) and significant negative autocorrelation at class midpoint distances of 77.6 km (I = − 0.679, *P* = 0.015) and 103.4 km (I = − 0.650, *P* = 0.025). Although significant autocorrelation signals were also detected at 252.2 km and 307.1 km, these distances exceeded the truncation threshold (145 km) used for PCNM construction. Consequently, the connectivity weights for these point pairs equal zero, indicating that these long-distance signals do not reflect the effective spatial scale of PCNM5. Accordingly, the maximum effective spatial scale of PCNM5 is 103.4 km.

Table 3
Moran's I statistics and significance levels for PCNM5 across distance classes.

Midpoint distances (km)	Moran's I	*P*	*n*
17.9	0.452	0.006**	53
43.9	−0.085	0.318	64
77.6	−0.679	0.015*	22
103.4	−0.650	0.025*	21
132.7	−0.193	0.318	12
162.5	−0.109	0.317	26
198.1	−0.062	0.447	18
225.1	−0.137	0.317	33
252.2	0.660	0.005**	28
286.7	−0.088	0.433	13
307.1	−0.899	0.035*	10

The distances are binned into 30 km intervals (e.g., 17.9 km corresponds to the 0–30 km range; 77.6 km to 60–90 km; 103.4 km to 90–120 km). The midpoint distance represents the arithmetic mean of all pairwise population distances within each bin. *P* values were corrected for each distance category via the Benjamini–Hochberg method. *$P < 0.05$, **$P < 0.01$, ***$P < 0.001$. *n* denotes the number of population pairs per bin. The truncation threshold (145 km) represents the maximum distance at which all populations remain connected within the PCNM weighting matrix.

Second, to exclude the possibility that this spatial structure is driven solely by measured environmental gradients, a partial Mantel test was performed (Table 4). With the environmental distance matrix (MAP, CEC, SC, Elev) controlled for, the correlation between the PCNM5 distance and the leaf anatomical trait distance was examined. The results revealed a significant positive correlation ($r = 0.229$, $P = 0.028$), indicating that the spatial structure captured by PCNM5 retains independent explanatory power for trait variation after accounting for environmental effects. Combined with the Moran's I results, PCNM5 effectively captures spatial autocorrelation at scales ≤ 103.4 km, and this structure cannot be fully explained by the measured environmental variables.

Table 4
Results of the partial Mantel test.

Mantel statistic r	*P*	Number of permutations
0.229	0.028	9999

Based on 25 populations of *P. zhennan*, a partial Mantel test was used to examine the correlation between the PCNM5 distance matrix and the distance matrix of leaf anatomical traits, while controlling for the environmental distance matrix. *P* values were from one-sided tests (alternative hypothesis: Mantel r > 0). Significance was assessed using 9,999 permutations.

4 Discussion

4.1 Modular differentiation and genetic constraints of leaf anatomical traits

The final phenotypes of leaf traits reflect the combined effects of genetic background and environmental selection [13, 51]. Research on the genes of *P. zhennan* has demonstrated that populations of this species still maintain a high level of genetic variation, which is mainly partitioned within populations, with moderate genetic differentiation among populations [41]. The anatomical evidence obtained in this study is highly consistent with the above findings: significant differences were observed in the degree of phenotypic variation and population differentiation across leaf anatomical traits; the coefficients of variation (CV) and phenotypic differentiation coefficient (PST) of individual traits ranged from 0.152 to 0.307 (Table 2) and from 0.05 to 0.51 (Fig. 2), respectively. Climatic, soil, and spatial factors together explained 33.9–76.4% of the trait variation (Fig. 4). These findings indicate that *P. zhennan* populations have retained abundant genetic variation to adapt to highly heterogeneous karst habitats. Furthermore, anatomical traits belonging to different functional modules experienced divergent environmental selection pressures during population differentiation.

Protective module traits (UET and LET) generally presented high variability and population differentiation, with CV ≥ 0.292 and PST ≥ 0.28. This pattern aligns well with the functional role of the leaf epidermis. As the direct interface between plants and the external environment, epidermal tissue serves as the primary defensive barrier against water loss, intense radiation, and habitat fluctuations [3]; its phenotype is expected to be relatively sensitive to environmental fluctuations for coping with stress. Within the conduction module, MVBW, as a core structure directly involved in water translocation, also exhibited pronounced environmental sensitivity and was significantly correlated with CEC, SC, and PCNM5 (Fig. 5); however, the magnitude of variation was modest (CV = 0.184, PST = 0.17). This is because its diameter is constrained by a trade-off between hydraulic safety and transport efficiency: an excessively large diameter increases the risk of embolism [52], whereas an excessively small diameter significantly increases hydraulic resistance. According to the Hagen–Poiseuille law, the resistance within a vascular conduit scales inversely with the fourth power of the conduit diameter [53]; consequently, MVBW is confined to a narrow range of functionally viable phenotypes and cannot deviate substantially. In contrast, the LPFT and PVD—which reflect the degree of vein reinforcement and the distribution density of primary veins [52, 54]—exhibit high variability and differentiation (CV ≥ 0.280, PST ≥ 0.39), which is consistent with the protective module. This finding indicates that in heterogeneous karst habitats, given

the constraint of the hydraulic safety–efficiency trade-off on the main vein width, *P. zhennan* tends to strengthen hydraulic conduction and mechanical support by increasing the PVD and thickening the LPFT.

Similarly, significant variation and population differentiation were also observed within the photosynthetic module. The LTT is a key indicator reflecting the density of palisade tissue arrangement; its magnitude correlates with the diffusion path length of CO_2 within the mesophyll: the higher the LTT is, the denser the palisade tissue and the shorter the intracellular CO_2 diffusion distance; conversely, the lower the LTT is, the longer the diffusion distance [7, 55]. In this study, LTT exhibited low variability and moderate population differentiation (CV = 0.152, PST = 0.19) and was generally constrained to a narrow viable range; nevertheless, significant interpopulation differences still existed within this range (P = 0.017), indicating its capacity for fine-scale phenotypic tuning across large-scale environmental gradients. In contrast, ST and PT/ST displayed high variability (CV ≥ 0.263) but the lowest degree of population differentiation (PST ≤ 0.1). Previous studies have demonstrated that palisade and spongy tissue thicknesses, as well as their ratios, strongly modulate foliar light absorption and gas exchange efficiency [15, 55]. Their high variability may stem primarily from individual phenotypic responses to local microenvironment conditions (such as canopy light position and microhydrology) but may not drive significant adaptive differentiation among populations under large-scale environmental selection.

Notably, the PST estimated in this study on the basis of field data incorporates both genetic differentiation and environmental plasticity [56, 57], and these two components cannot be quantitatively separated. Although Liang et al. reported moderate genetic differentiation among *P. zhennan* populations [41], the respective contributions of genetics and plasticity to interpopulation divergence in leaf anatomical traits remain to be quantified via common garden experiments or QST–FST comparisons. A meta-analysis demonstrated that plasticity, on average, dominates phenotypic divergence between populations and is frequently positively correlated with genetic differentiation[58]. However, in some cases, plasticity is negatively correlated with genetic differentiation or even exhibits non-adaptive patterns [58]. These findings suggest that interpopulation differences in the leaf anatomical traits of *P. zhennan* largely reflect adaptive responses to heterogeneous karst habitats. Nevertheless, the relative contributions of plasticity and genetic differentiation require further experimental partitioning.

4.2 Environmental and spatial drivers of leaf anatomical trait variation

Numerous studies have demonstrated significant variations in plant leaf traits at large spatial scales, with elevation, climate, and soil factors widely recognized as crucial determinants of leaf trait variation in plants [15, 59]. This conclusion was also verified in the present study: 44.8% of trait variation could be collectively explained by soil factors (20.3%), spatial factors (18.2%), and climatic factors (13.6%) (Fig. 3b). Specifically, the variation in the protective module (UET, LET) was jointly regulated by soil and climatic factors; the variation in the conductive module (LPFT, MVBW, and PVD) was driven primarily by soil and spatial factors. With respect to the photosynthetic module, ST was influenced mainly by spatial factors, whereas LTT and PT/ST were governed predominantly by soil and spatial factors and climatic

and spatial factors, respectively (Fig. 4). In addition, previous studies have generally confirmed that soil properties (e.g., moisture and nutrients) are highly dependent on the climatic context [60]; consequently, climatic factors typically explain a greater proportion of leaf trait variation than do soil factors [61], and trait variation is generally driven more by the interactive effects of climate and soil rather than their independent main effects [15]. Nevertheless, an opposite pattern was detected in karst regions: the pronounced soil heterogeneity unique to karst habitats acts as the core driver of leaf trait variation, supporting the view that soil factors constitute the primary limiting factor for plant growth and development in karst regions [15, 42, 43]. Notably, trait responses to soil, climatic, and spatial factors were dominated by independent main effects, whereas interactive effects among these environmental drivers were nearly insignificant. This pattern likely stems from unique geological features of karst characteristics, including bedrock fissures and shallow, discontinuous soil layers [42, 43]. Crucially, single-factor hierarchical partitioning further revealed that the spatial variable PCNM5 accounted for the largest unique contribution (23.88%) (Fig. 3c). Together with its significant spatial autocorrelation range of 103.4 km (Table 3), this finding implies that leaf trait variation within *P. zhennan* populations is driven by both environmental filtering and complex spatial structures [47].

4.3 Scale effects in spatial autocorrelation

Spatial autocorrelation (SAC) describes the nonindependence of observations among geographically adjacent sampling sites. Its sources include biological processes (e.g., dispersal and competition) as well as unmeasured environmental variables with inherent spatial structure [62]; the latter is commonly referred to as spatial dependence [63]. Generally, such correlational patterns vary dynamically across spatial scales. Positive autocorrelation among similar neighboring units frequently emerges at fine scales, whereas negative autocorrelation between dissimilar units prevails at broader scales, with such patterns spanning spatial extents from micrometers to hundreds of kilometers [64]. In this study, principal coordinates of neighborhood matrices (PCNM) [46, 47] were used to generate spatial eigenvectors for quantifying spatial autocorrelation (SAC). The significant spatial vector PCNM5 was included as a predictor in subsequent statistical models. The partial Mantel test revealed that the spatial structure captured by PCNM5 explains a significant independent fraction of trait variation after accounting for environmental effects. These findings confirm the pivotal role of spatial structure in shaping leaf anatomical trait variation and highlight the importance of explicitly incorporating spatial autocorrelation during analyses of plant traits within karst landscapes.

The spatial autocorrelation pattern of PCNM5 varied substantially with midpoint distance, indicating that dominant ecological processes fundamentally differ across scales (Table 3). At a class midpoint distance of 17.9 km, PCNM5 exhibited strong positive autocorrelation (I = 0.452, P = 0.006), indicating marked similarity in spatial structure among proximate populations. This likely reflects limited seed dispersal, whereby adjacent populations retain high trait homogeneity [47]. However, at class midpoint distances of 77.6 km and 103.4 km, PCNM5 shifted to significant negative autocorrelation (I = − 0.679, P = 0.015; I = − 0.650, P = 0.025), revealing pronounced spatial divergence at broader scales. This pattern may arise from geographic isolation restricting interpopulation gene flow, which allows populations

across discrete spatial units to accumulate genetic divergence over long-term evolution [41], or from spatially structured but unmeasured environmental variables [62].

4.4 Adaptive strategies for determining leaf anatomical traits across environmental and spatial gradients

Model comparisons revealed that the ΔAIC values for some traits were less than 2 (see Additional file 2), indicating that the linear model and the GAM exhibited comparable fitting performance. However, the ΔAIC values for UET, LET, MVBW, and PT/ST all exceeded 2, with the value for LET reaching 10.36. Following previously established criteria [50], GAM provide a more appropriate fit for these traits. The response patterns of leaf anatomical traits were further elucidated via generalized additive models (GAM), revealing distinct strategies across functional modules. Within the protective module, both UET and LET exhibited nonlinear responses to MAP (Fig. 5a, b). Epidermal thickness increased significantly at the high-moisture end (> 1,150 mm), suggesting that excessive moisture triggers increased epidermal investment. No clear trend in epidermal thickness was observed below this threshold. Although epidermal thickening is widely recognized as a typical strategy to cope with drought stress [65–67]—implying that epidermal thickness might follow a U-shaped curve across broader precipitation gradients—the present results indicate that within the karst-adapted precipitation range, epidermal investment is driven primarily by high moisture availability, reflecting a cost-optimization strategy adopted by the protective module within specific precipitation ranges. Furthermore, LET exhibited a nonlinear response to the soil factor CEC, increasing initially and then plateauing (Fig. 5c), which aligns with leaf economic spectrum theory [3]: high CEC alleviates nutrient limitation, permitting greater investment in epidermal tissues, yet the mechanistic benefits eventually saturate. Conversely, the linear increase in LET with increasing SC (Fig. 5d) suggests that, in sandy substrates, the lower epidermis—as the interface in contact with the soil—must increase its physical resistance to mitigate abrasive damage. Notably, LET exhibited a U-shaped response to PCNM5 (Fig. 5e). Combined with the scale-dependent autocorrelation patterns discussed above, this likely reflects genetic differentiation driven by long-term geographic isolation at distances of 77.6–103.4 km or responses to unmeasured, spatially structured environmental variables that collectively impose selective pressures on epidermal investment.

Within the conductive module, MVBW exhibited a nonlinear response to PCNM5, initially increasing and subsequently plateauing (Fig. 5j). This finding suggests that MVBW is modulated by genetic differentiation or unmeasured spatially structured environmental factors, resulting in a distinct threshold effect: once PCNM5 exceeds this threshold, the phenotypic plasticity of vascular bundle width tends to saturate. In contrast, MVBW showed a significant negative linear relationship with SC (Fig. 5i). This aligns with the expectation that sandy soils feature low water availability and intense environmental fluctuations; under such conditions, overly wide vessels are prone to air embolism [15, 52]. Consequently, plants adopt a conservative strategy that prioritizes hydraulic safety over transport efficiency [52]. This adaptive mechanism is further corroborated by the positive linear relationship between LPFT and SC, demonstrating that plants enhance mechanical support by thickening phloem fibers in sandy substrates. Both MVBW and PVD exhibited negative linear responses to the CEC (Fig. 5h, k). These findings indicate

that under conditions of low cation exchange capacity, the width of the vascular bundle increases, and the density of the primary vein increases to improve overall water and solute transport efficiency, thereby sustaining metabolic activity [53, 54]. Additionally, LPFT increased linearly with MAP (Fig. 5f); this trend likely reflects elevated biomechanical demands for structural stability in humid climates, where expanded leaf areas require stronger midrib mechanical support [5].

Within the photosynthetic module, all the traits presented linear responses. Palisade tissue comprises tightly packed cells; thicker palisade layers contain more chloroplasts, thereby enhancing light capture and potential photosynthetic capacity [68]. Conversely, spongy tissue possesses large intercellular airspaces that facilitate gaseous diffusion [13]. Furthermore, the irregular morphology of spongy mesophyll cells enhances light scattering and multiple scattered light absorption, further optimizing photosynthetic efficiency [7]. In this study, PT/ST increased linearly with MAP (Fig. 5m), whereas LTT also rose linearly with SC and elevation (Fig. 5o, p). These findings indicate that, under humid conditions, on sandy substrates, or at high altitudes, *P. zhennan* tends to augment chloroplast allocation to increase light harvesting and increase its photosynthetic potential. Notably, PT/ST decreased linearly with PCNM5 (Fig. 5n), whereas ST increased linearly with PCNM5 (Fig. 5l). This coordinated shift suggests that, under genetic differentiation or spatially structured environmental stressors operating at scales of 77.6–103.4 km, plants optimize gaseous exchange and light absorption by reallocating biomass from palisade to spongy tissues. Notably, the optimization of the photosynthetic architecture is inherently constrained by physiological thresholds, such as the light saturation point and CO_2 saturation point [69]. The predominance of linear responses observed here implies that the environmental gradients encompassed within the study area remain within the physiological tolerance limits of *P. zhennan*. This linear plasticity reflects the stable adaptive capacity of *P. zhennan* to heterogeneous karst habitats.

5 Conclusions

This study revealed the modular adaptive strategies of *P. zhennan* leaf traits in response to spatial structure, precipitation, and soil factors. Together, these three factors accounted for 44.8% of the total variation, with soil being the most significant factor. The protective, conductive, and photosynthetic modules exhibit three distinct response patterns, namely, nonlinear threshold response, constrained trade-off, and linear optimization, respectively, highlighting the necessity of considering functional specialization in karst adaptation. Future research should extend this modular adaptation framework to other karst-endemic woody plants and integrate genetic analyses with common garden experiments to further elucidate the evolutionary basis and conservation implications of trait adaptation.

Abbreviations

Abbreviation	Full form
UCT	upper cuticle thickness
UET	upper epidermis thickness
LET	lower epidermis thickness
PT	palisade tissue thickness
ST	spongy tissue thickness
LT	leaf thickness
MVBW	main vein vascular bundle width
MVBT	main vein vascular bundle thickness
MVXT	main vein xylem thickness
UPFT	upper phloem fiber thickness in the main vein
LPFT	lower phloem fiber thickness in the main vein
PVD	primary vein density
MD/MT	main vein diameter–thickness ratio
PT/ST	palisade–sponge ratio
LTT	tightness of the leaf tissue structure
LTL	looseness of the leaf tissue structure
MAP	mean annual precipitation
MAT	mean annual temperature
≥ 0°C AT	≥ 0°C accumulated temperature
≥ 10°C AT	≥ 10°C accumulated temperature
RH	relative humidity
TOC	total organic carbon
SC	sand content
CC	clay content
CEC	cation exchange capacity
TN	total nitrogen
Elev	elevation
PCNM	principal coordinates of neighborhood matrices

Abbreviation	Full form
VIF	variance inflation factors
LMM	linear mixed model
VPA	variation partitioning analysis
CR	covariance ratio
PST	phenotypic differentiation coefficient
RDA	redundancy analysis
GAM	generalized additive model
LM	linear model
AIC	Akaike information criterion
REML	restricted maximum likelihood

Declarations

Ethics approval and consent to participate

Not applicable

Consent for publication

Not applicable

Availability of data and materials

The data supporting the findings of this study are available within the article and its Supplementary Material. Additional data are available from the corresponding author upon reasonable request.

Competing interests

The authors declare that the research was conducted in the absence of any commercial or financial relationships that could be construed as potential conflicts of interest.

Funding

This research was supported by the Guizhou Provincial Key Technology R&D Program (QianKeHeZhiCheng [2023] No. 187), the Guizhou Provincial Basic Research Program (Natural Science) (QianKeHeJiChu QN[2025]381), the Innovative Talent Team Project of Seedling Breeding and Plantation Cultivation for Precious Tree Species in Guizhou (Qiankehe Platform Talents -CXTD[2023]006), the

National Natural Science Foundation of China (NSFC) (Grant No. 32501450), and the Key Research Project of the Guizhou Forestry Bureau (QLKH [2026] ZD004).

Authors' contributions

EnYi Dai: Conceptualization, methodology, writing - original draft, and visualization. **Hong Luo:** Writing - Review & editing, funding acquisition, supervision, project administration, methodology. **HengFeng Jia:** Writing - Review & editing, supervision. **ShaSha Wang:** Writing - Review & editing, supervision. **YunLi Jiang:** Writing - Review & editing, supervision. **YanBing Yang:** Writing - Review & editing, supervision. **FengXia Yan:** Writing - Review & editing, supervision.

Acknowledgments

Not applicable.

References

1. Poorter H, Niinemets U, Poorter L, Wright IJ, Villar H. Causes and consequences of variation in leaf mass per area (LMA): a meta-analysis. New Phytologist. 2009;182:565–88. https://doi.org/10.1111/j.1469-8137.2009.02830.x.
2. Klich MG. Leaf variations in Elaeagnus angustifolia related to environmental heterogeneity. Environ Exp Bot. 2000;44:171–83. https://doi.org/10.1016/s0098-8472(00)00056-3.
3. Wright IJ, Reich PB, Westoby M, Ackerly DD, Baruch Z, Bongers F, et al. The worldwide leaf economics spectrum. Nature. 2004;428:821–7. https://doi.org/10.1038/nature02403.
4. Ni X, Sun L, Cai Q, Ma S, Feng Y, Sun Y, et al. Variation and determinants of leaf anatomical traits from boreal to tropical forests in eastern China. Ecological Indicators. 2022;140:108992. https://doi.org/10.1016/j.ecolind.2022.108992.
5. Soheili F, Heydari M, Woodward S, Naji HR. Adaptive mechanism in Quercus brantii Lindl. leaves under climatic differentiation: morphological and anatomical traits. Sci Rep. 2023;13:3580. https://doi.org/10.1038/s41598-023-30762-1.
6. Meletiou-Christou MS, Rhizopoulou S, Diamantoglou S. Seasonal changes of carbohydrates, lipids and nitrogen content in sun and shade leaves from four mediterranean evergreen sclerophylls. Environmental and Experimental Botany. 1994;34:129–40. https://doi.org/10.1016/0098-8472(94)90032-9.
7. Terashima I, Hanba YT, Tholen D, Niinemets Ü. Leaf Functional Anatomy in Relation to Photosynthesis. Plant Physiology. 2011;155:108–16. https://doi.org/10.1104/pp.110.165472.
8. Chen L, Wang R. Anatomical and physiological divergences and compensatory effects in two *Leymus chinensis* (Poaceae) ecotypes in Northeast China. Agriculture, Ecosystems & Environment. 2009;134:46–52. https://doi.org/10.1016/j.agee.2009.05.015.

9. Santos KR, Pereira MP, Ferreira ACG, Rodrigues LC de A, Castro EM de, Corrêa FF, et al. *Typha domingensis* Pers. growth responses to leaf anatomy and photosynthesis as influenced by phosphorus. Aquatic Botany. 2015;122:47–53. https://doi.org/10.1016/j.aquabot.2015.01.007.
10. Cai Q, Ji C, Yan Z, Jiang X, Fang J. Anatomical responses of leaf and stem of Arabidopsis thaliana to nitrogen and phosphorus addition. J Plant Res. 2017;130:1035–45. https://doi.org/10.1007/s10265-017-0960-2.
11. Givnish TJ. Ecological constraints on the evolution of plasticity in plants. Evolutionary Ecology. 2002;16:213–42. https://doi.org/10.1023/A:1019676410041.
12. Aguraijuja K, Klõšeiko J, Ots K, Lukjanova A. Effect of wood ash on leaf and shoot anatomy, photosynthesis and carbohydrate concentrations in birch on a cutaway peatland. Environ Monit Assess. 2015;187:444. https://doi.org/10.1007/s10661-015-4681-5.
13. He N, Liu C, Tian M, Li M, Yang H, Yu G, et al. Variation in leaf anatomical traits from tropical to cold-temperate forests and linkage to ecosystem functions. Functional Ecology. 2018;32:10–9. https://doi.org/10.1111/1365-2435.12934.
14. Diemer M. Life span and dynamics of leaves of herbaceous perennials in high-elevation environments: 'news from the elephant's leg.' Functional Ecology. 1998;12:413–25. https://doi.org/10.1046/j.1365-2435.1998.00207.x.
15. Shao S, Li G, Wang J, Wang Y, Qu M, Zhao H, et al. Temperature and soil attributes drive the regional variation in leaf anatomical traits of *Populus euphratica*. Global Ecology and Conservation. 2024;54:e03107. https://doi.org/10.1016/j.gecco.2024.e03107.
16. Ordoñez JC, Van Bodegom PM, Witte JM, Wright IJ, Reich PB, Aerts R. A global study of relationships between leaf traits, climate and soil measures of nutrient fertility. Global Ecology and Biogeography. 2009;18:137–49. https://doi.org/10.1111/j.1466-8238.2008.00441.x.
17. Sun D, Gao C, Song Q, Wan X, Nie Y, Wang Q. Relationship between leaf anatomical structure of Camellia oleifera and drought tolerance in high-altitude regions. Guihaia. 2025;45:2184–99.
18. Pigliucci M. Phenotypic integration: studying the ecology and evolution of complex phenotypes. Ecology Letters. 2003;6:265–72. https://doi.org/10.1046/j.1461-0248.2003.00428.x.
19. Li Y, Liu C, Sack L, Xu L, Li M, Zhang J, et al. Leaf trait network architecture shifts with species-richness and climate across forests at continental scale. Ecology Letters. 2022;25:1442–57. https://doi.org/10.1111/ele.14009.
20. Li X, Li Z, Xu Z, Lu Z, Fan Z, Chen Y, et al. Leaf trait networks shift toward high modularity during the succession of a subtropical forest, in southwest China. Ecological Indicators. 2024;166:112490. https://doi.org/10.1016/j.ecolind.2024.112490.
21. Armbruster WS, Pélabon C, Bolstad GH, Hansen TF. Integrated phenotypes: understanding trait covariation in plants and animals. Philos Trans R Soc Lond B Biol Sci. 2014;369:20130245. https://doi.org/10.1098/rstb.2013.0245.
22. Klingenberg CP. Studying morphological integration and modularity at multiple levels: concepts and analysis. Philos Trans R Soc Lond B Biol Sci. 2014;369:20130249.

https://doi.org/10.1098/rstb.2013.0249.

23. De Kroon H, Huber H, Stuefer JF, Van Groenendael JM. A modular concept of phenotypic plasticity in plants. New Phytologist. 2005;166:73–82. https://doi.org/10.1111/j.1469-8137.2004.01310.x.
24. Evans KM, Felice R. Integration and modularity and their role in speciation and evolutionary diversification. Nat Rev Biodivers. 2026;2:457–66. https://doi.org/10.1038/s44358-026-00175-9.
25. Díaz S. Plant functional traits and the entangled phenotype. Functional Ecology. 2025;39:1144–59. https://doi.org/10.1111/1365-2435.70017.
26. Xing K, Niinemets Ü, Rengel Z, Onoda Y, Xia J, Chen HYH, et al. Global patterns of leaf construction traits and their covariation along climate and soil environmental gradients. New Phytologist. 2021;232:1648–60. https://doi.org/10.1111/nph.17686.
27. Yang H, Zhang Z-Q, Ding J, Li L, Tang Y-Y, Feng J-C, et al. Contrasting trait variations and trait correlation networks across heteromorphic leaves of Populus euphratica. J Plant Ecol. 2025;18:rtaf025. https://doi.org/10.1093/jpe/rtaf025.
28. Matesanz S, Blanco-Sánchez M, Ramos-Muñoz M, de la Cruz M, Benavides R, Escudero A. Phenotypic integration does not constrain phenotypic plasticity: differential plasticity of traits is associated to their integration across environments. New Phytologist. 2021;231:2359–70. https://doi.org/10.1111/nph.17536.
29. Stotz GC, Salgado-Luarte C, Escobedo VM, Gianoli E. Phenotypic integration limits the variation in plant phenotypic plasticity among traits: A meta-analysis. Functional Ecology. 2025;39:3021–33. https://doi.org/10.1111/1365-2435.70096.
30. Lin Y, Kuang L, Tang S, Mou Z, Phillips OL, Lambers H, et al. Leaf traits from stomata to morphology are associated with climatic and edaphic variables for dominant tropical forest evergreen oaks. Journal of Plant Ecology. 2021;14:1115–27. https://doi.org/10.1093/jpe/rtab060.
31. Guo W, Cherubini P, Zhang J, Hu X, Li M, Qi L. Soil physicochemical properties determine leaf traits but not size traits of moso bamboo (Phyllostachys edulis). Environ Res Lett. 2022;17:114061. https://doi.org/10.1088/1748-9326/aca039.
32. Sandel B, Griffin-Nolan RJ. Idiosyncrasy and predictability in intraspecific trait–climate relationships of grasses. Ecosphere. 2024;15:e4828. https://doi.org/10.1002/ecs2.4828.
33. Zhu H, Wang C, Xie Y, Ma L, Chen B. Effects of substrate on growth and photosynthetic physiology of Phoebe zhennan seedlings. Journal of Southwest University (Natural Science Edition). 2021;43:27–34. https://doi.org/10.13718/j.cnki.xdzk.2021.05.004.
34. Peng J, Xie J, Gu Y, Guo H, Zhang S, Huang X, et al. Assessing population genetic structure and diversity and their driving factors in Phoebe zhennan populations. BMC Plant Biol. 2024;24:1091. https://doi.org/10.1186/s12870-024-05810-1.
35. Tariq A, Pan K, Olatunji OA, Graciano C, Li Z, Sun F, et al. Phosphorous Application Improves Drought Tolerance of Phoebe zhennan. Front Plant Sci. 2017;8:1561. https://doi.org/10.3389/fpls.2017.01561.

36. Hu Y, Wang B, Hu T, Chen H, Li H, Zhang W, et al. Combined action of an antioxidant defence system and osmolytes on drought tolerance and post-drought recovery of Phoebe zhennan S. Lee saplings. Acta Physiol Plant. 2015;37:84. https://doi.org/10.1007/s11738-015-1831-x.
37. Ou H, Lin J, Li J, Liang R. Variation in leaf phenotypic traits of Phoebe zhennan from different provenances. Southwest China Journal of Agricultural Sciences. 2020;33:637–44. https://doi.org/10.16213/j.cnki.scjas.2020.3.026.
38. Liang J, Mao H, Guo L, Fu Y, Wu F, Zhang J, et al. Effects of shading on growth and photosynthesis of seedlings of three valuable native broadleaf tree species. Journal of Northwest Forestry University. 2019;34:57–63.
39. Li G, Zhu Y, Zhou S, Lu Y, Zhang J, Tong Z. Physiological responses to low-temperature stress and cold tolerance in two leaf-type varieties of Phoebe zhennan. Journal of Zhejiang A & F University. 2017;34:310–8.
40. Chen Z, Xue X, Cheng R, Wu H, Gao H, Gao Z. Geographical origin classification of Phoebe zhennan and Phoebe bournei by solid phase micro-extraction and gas chromatography-mass spectrometry. J Wood Sci. 2023;69:21. https://doi.org/10.1186/s10086-023-02095-0.
41. Liang Q, Jia Y, Shi R, Zhao D, Luo M. Development and characterization of SSR markers in Phoebe zhennan. PeerJ. 2025;13:e20434. https://doi.org/10.7717/peerj.20434.
42. Huang K, Ma Z, Wang X, Shan J, Zhang Z, Xia P, et al. Control of soil organic carbon under karst landforms: A case study of Guizhou Province, in southwest China. Ecological Indicators. 2022;145:109624. https://doi.org/10.1016/j.ecolind.2022.109624.
43. Chen H, Nie Y, Wang K. Spatiotemporal heterogeneity of water and plant adaptation mechanisms in karst mountain areas: a review. Acta Ecologica Sinica. 2013;33:317–26.
44. China Meteorological Data Network. https://data.cma.cn/. Accessed 1 Nov 2025.
45. Harmonized World Soil Database version 2.0 (HWSD v2.0). https://gaez.fao.org/pages/hwsd. Accessed 1 Nov 2025.
46. Borcard D, Legendre P. All-scale spatial analysis of ecological data by means of principal coordinates of neighbour matrices. Ecological Modelling. 2002;153:51–68. https://doi.org/10.1016/S0304-3800(01)00501-4.
47. Dray S, Legendre P, Peres-Neto PR. Spatial modelling: a comprehensive framework for principal coordinate analysis of neighbour matrices (PCNM). Ecological Modelling. 2006;196:483–93. https://doi.org/10.1016/j.ecolmodel.2006.02.015.
48. Dormann CF, Elith J, Bacher S, Buchmann C, Carl G, Carré G, et al. Collinearity: a review of methods to deal with it and a simulation study evaluating their performance. Ecography. 2013;36:27–46. https://doi.org/10.1111/j.1600-0587.2012.07348.x.
49. Adams DC. Evaluating modularity in morphometric data: challenges with the RV coefficient and a new test measure. Methods Ecol Evol. 2016;7:565–72. https://doi.org/10.1111/2041-210X.12511.
50. Symonds MRE, Moussalli A. A brief guide to model selection, multimodel inference and model averaging in behavioural ecology using Akaike's information criterion. Behav Ecol Sociobiol.

2011;65:13–21. https://doi.org/10.1007/s00265-010-1037-6.

51. An J, Huo H, Liu Q, Jiang Y, Luo H, Hao Y. Physiological and molecular mechanisms of nitrogen in alleviating drought stress in Phoebe bournei. Sci Rep. 2025;15:14684. https://doi.org/10.1038/s41598-025-99312-1.
52. Sack L, Scoffoni C. Leaf venation: structure, function, development, evolution, ecology and applications in the past, present and future. New Phytologist. 2013;198:983–1000. https://doi.org/10.1111/nph.12253.
53. Coomes DA, Heathcote S, Godfrey ER, Shepherd JJ, Sack L. Scaling of xylem vessels and veins within the leaves of oak species. Biol Lett. 2008;4:302–6. https://doi.org/10.1098/rsbl.2008.0094.
54. Taneda H, Terashima I. Co-ordinated development of the leaf midrib xylem with the lamina in Nicotiana tabacum. Annals of Botany. 2012;110:35–45. https://doi.org/10.1093/aob/mcs102.
55. Evans JR, Kaldenhoff R, Genty B, Terashima I. Resistances along the CO2 diffusion pathway inside leaves. J Exp Bot. 2009;60:2235–48. https://doi.org/10.1093/jxb/erp117.
56. Merilä J, Crnokrak P. Comparison of genetic differentiation at marker loci and quantitative traits. Journal of Evolutionary Biology. 2001;14:892–903. https://doi.org/10.1046/j.1420-9101.2001.00348.x.
57. Schmid M, Guillaume F. The role of phenotypic plasticity on population differentiation. Heredity. 2017;119:214–25. https://doi.org/10.1038/hdy.2017.36.
58. Stamp MA, Hadfield JD. The relative importance of plasticity versus genetic differentiation in explaining between population differences; a meta-analysis. Ecology Letters. 2020;23:1432–41. https://doi.org/10.1111/ele.13565.
59. Li Y, Zou D, Shrestha N, Xu X, Wang Q, Jia W, et al. Spatiotemporal variation in leaf size and shape in response to climate. Journal of Plant Ecology. 2020;13:87–96. https://doi.org/10.1093/jpe/rtz053.
60. Parida AK, Das AB, Mittra B. Effects of salt on growth, ion accumulation, photosynthesis and leaf anatomy of the mangrove, Bruguiera parviflora. Trees. 2004;18:167–74. https://doi.org/10.1007/s00468-003-0293-8.
61. He J, Wang X, Schmid B, Flynn DFB, Li X, Reich PB, et al. Taxonomic identity, phylogeny, climate and soil fertility as drivers of leaf traits across Chinese grassland biomes. J Plant Res. 2010;123:551–61. https://doi.org/10.1007/s10265-009-0294-9.
62. Dormann CF, McPherson JM, Araújo MB, Bivand R, Bolliger J, Carl G, et al. Methods to account for spatial autocorrelation in the analysis of species distributional data: a review. Ecography. 2007;30:609–28. https://doi.org/10.1111/j.2007.0906-7590.05171.x.
63. Legendre P, Dale MRT, Fortin M-J, Gurevitch J, Hohn M, Myers D. The consequences of spatial structure for the design and analysis of ecological field surveys. Ecography. 2002;25:601–15. https://doi.org/10.1034/j.1600-0587.2002.250508.x.
64. Dormann CF. Effects of incorporating spatial autocorrelation into the analysis of species distribution data. Global Ecology and Biogeography. 2007a;16:129–38. https://doi.org/10.1111/j.1466-8238.2006.00279.x.

65. Hu Y, Yang L, Gao C, Liao D, Long L, Qiu J, et al. A comparative study on the leaf anatomical structure of Camellia oleifera in a low-hot valley area in Guizhou Province, China. PLOS ONE. 2022;17:e0262509. https://doi.org/10.1371/journal.pone.0262509.
66. Kosma DK, Bourdenx B, Bernard A, Parsons EP, Lü S, Joubès J, et al. The Impact of Water Deficiency on Leaf Cuticle Lipids of Arabidopsis. Plant Physiology. 2009;151:1918–29. https://doi.org/10.1104/pp.109.141911.
67. McDowell N, Pockman WT, Allen CD, Breshears DD, Cobb N, Kolb T, et al. Mechanisms of plant survival and mortality during drought: why do some plants survive while others succumb to drought? New Phytologist. 2008;178:719–39. https://doi.org/10.1111/j.1469-8137.2008.02436.x.
68. Chen B, Wang C, Tian Y, Chu Q, Hu C. Anatomical characteristics of young stems and mature leaves of dwarf pear. Sci Hortic. 2015;186:172–9. https://doi.org/10.1016/j.scienta.2015.02.025.
69. Chazdon RL, Pearcy RW, Lee DW, Fetcher N. Photosynthetic Responses of Tropical Forest Plants to Contrasting Light Environments. In: Mulkey SS, Chazdon RL, Smith AP, editors. Tropical Forest Plant Ecophysiology. Boston, MA: Springer US; 1996. p. 5–55. https://doi.org/10.1007/978-1-4613-1163-8_1.

Figures

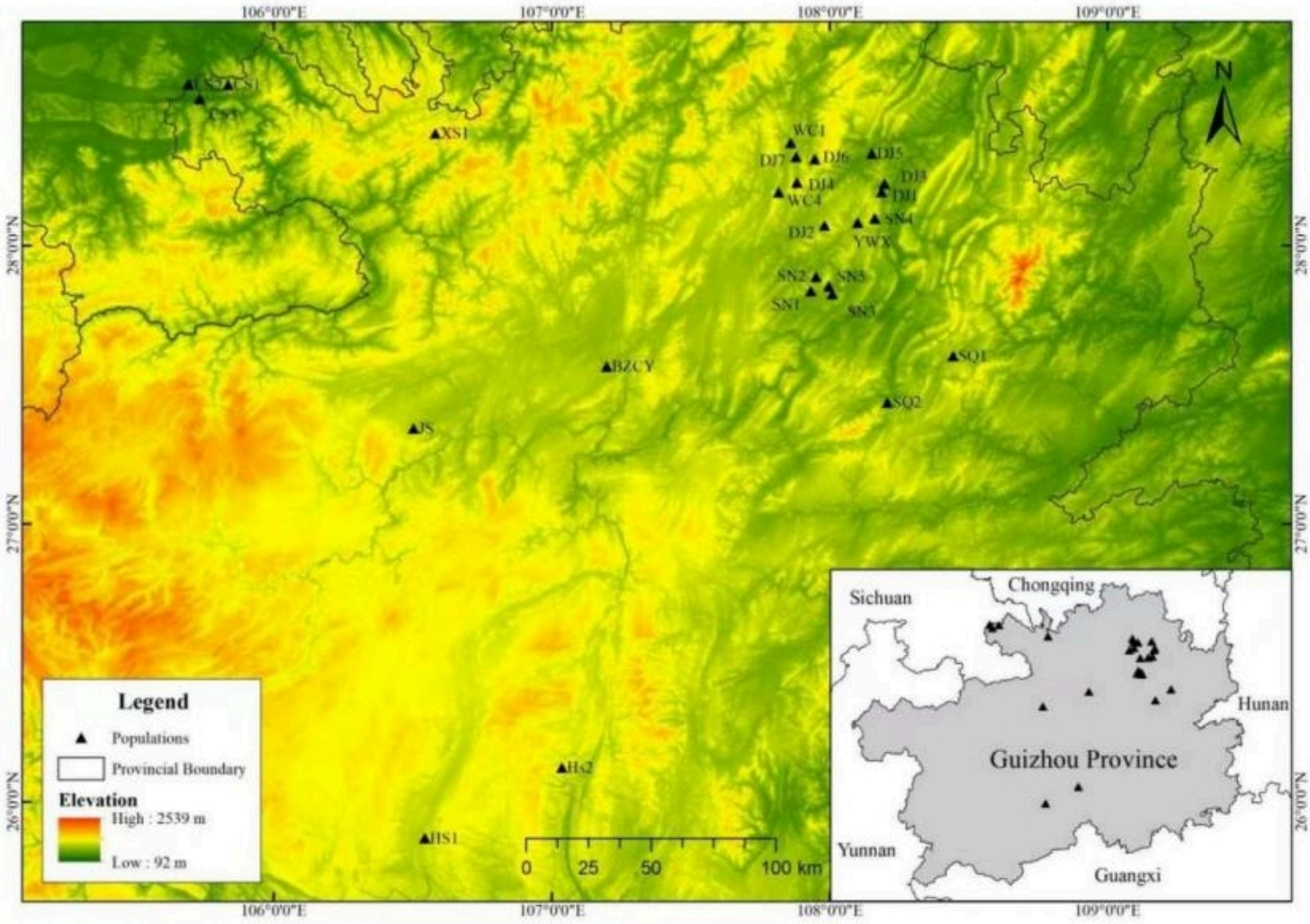

Figure 1

Distribution of 25 *P. zhennan* populations in the karst region of southwestern China.

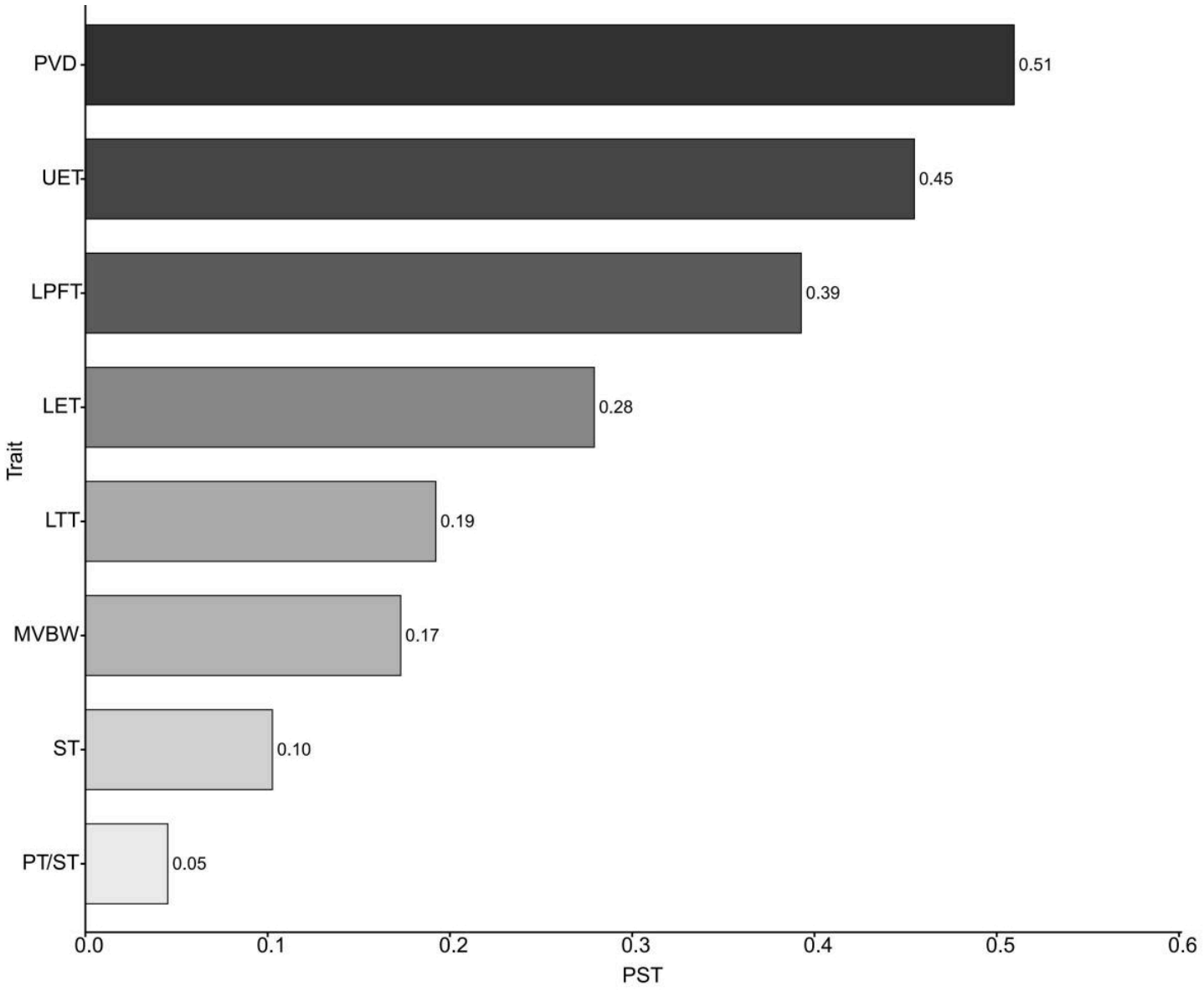

Figure 2

Phenotypic differentiation of leaf anatomical traits among *P. zhennan* populations. UET, upper epidermal thickness (μm); LET, lower epidermal thickness (μm); MVBW, main vein vascular bundle width (μm); LPFT, lower phloem fiber thickness in the main vein (μm); PVD, primary vein density (veins mm^{-1}); ST, spongy tissue thickness (μm); LTT, tightness of the leaf tissue structure; PT/ST, palisade–sponge ratio.

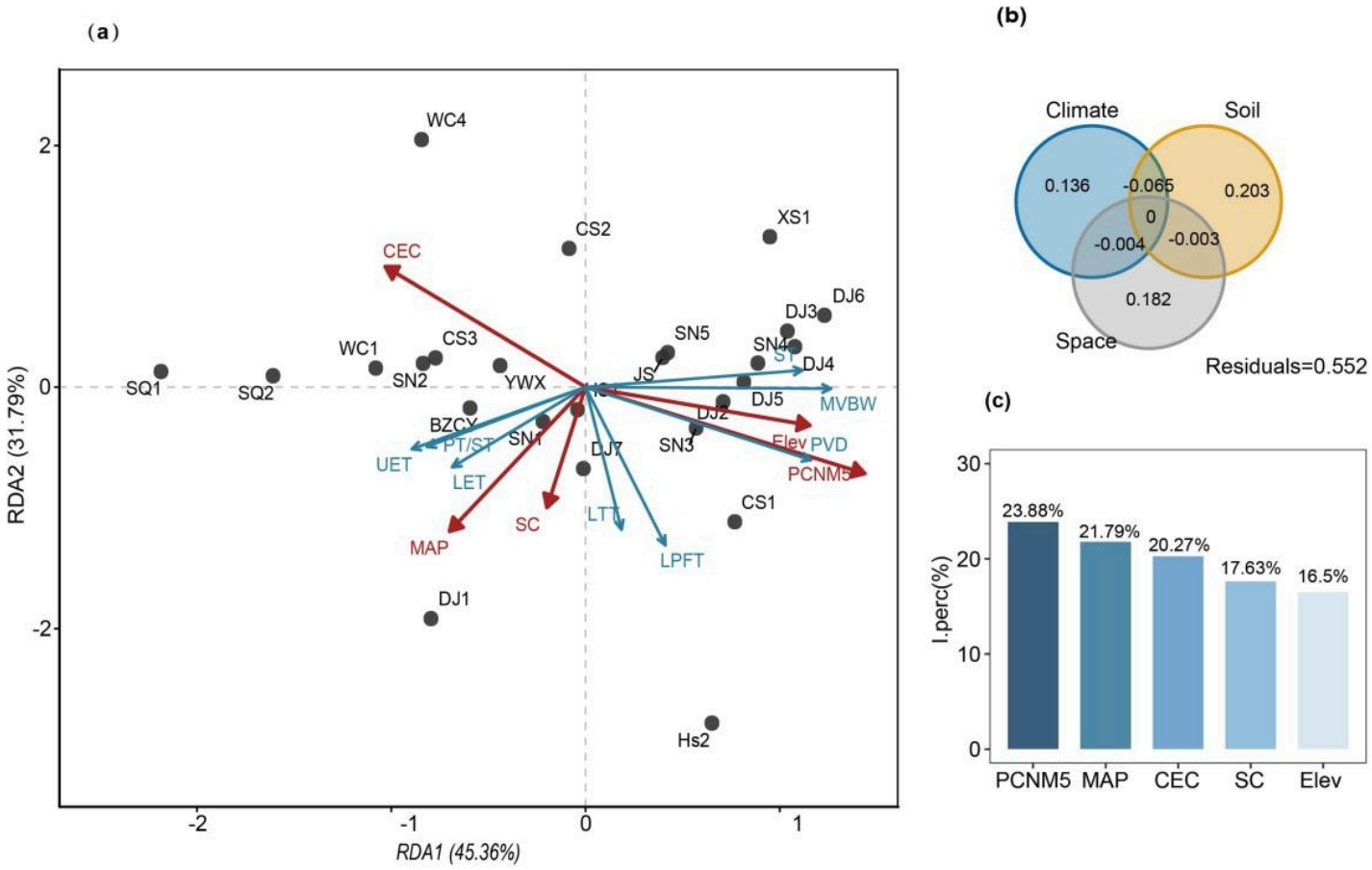

Figure 3

Determinants of leaf anatomical trait variation. (a) RDA ordination biplot showing relationships between leaf traits and environmental/space variables; (b) variance partitioning of climatic, soil, and spatial factors; (c) relative contributions of individual predictor variables. The blackdots represent individual populations; abbreviations follow those in Fig. 2.

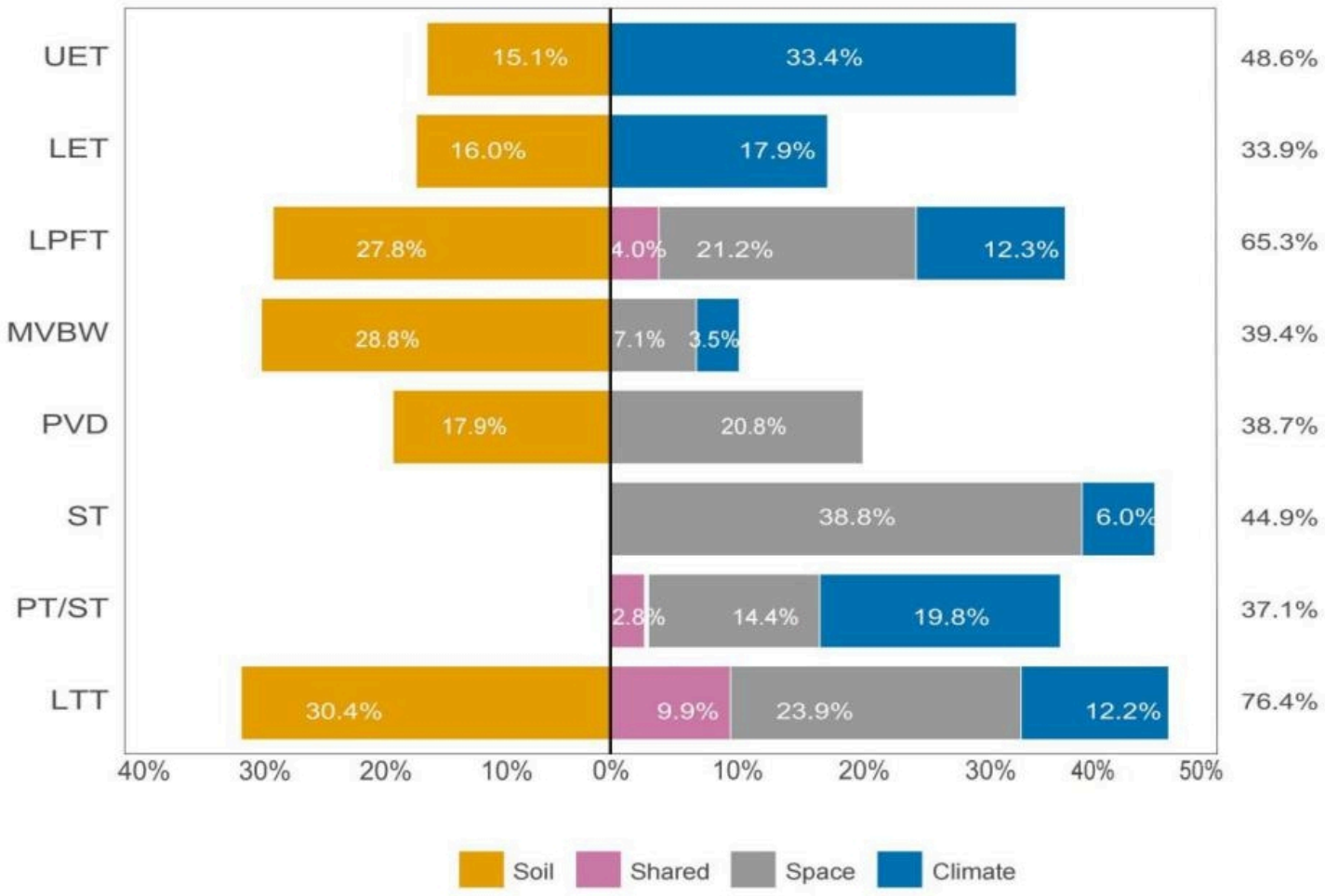

Figure 4

Variance partitioning of individual leaf anatomical traits. The values represent the adjusted R^2 from variation partitioning analysis (VPA). The negativeadjusted R^2 values were set to zero. Abbreviations follow those in Fig. 2.

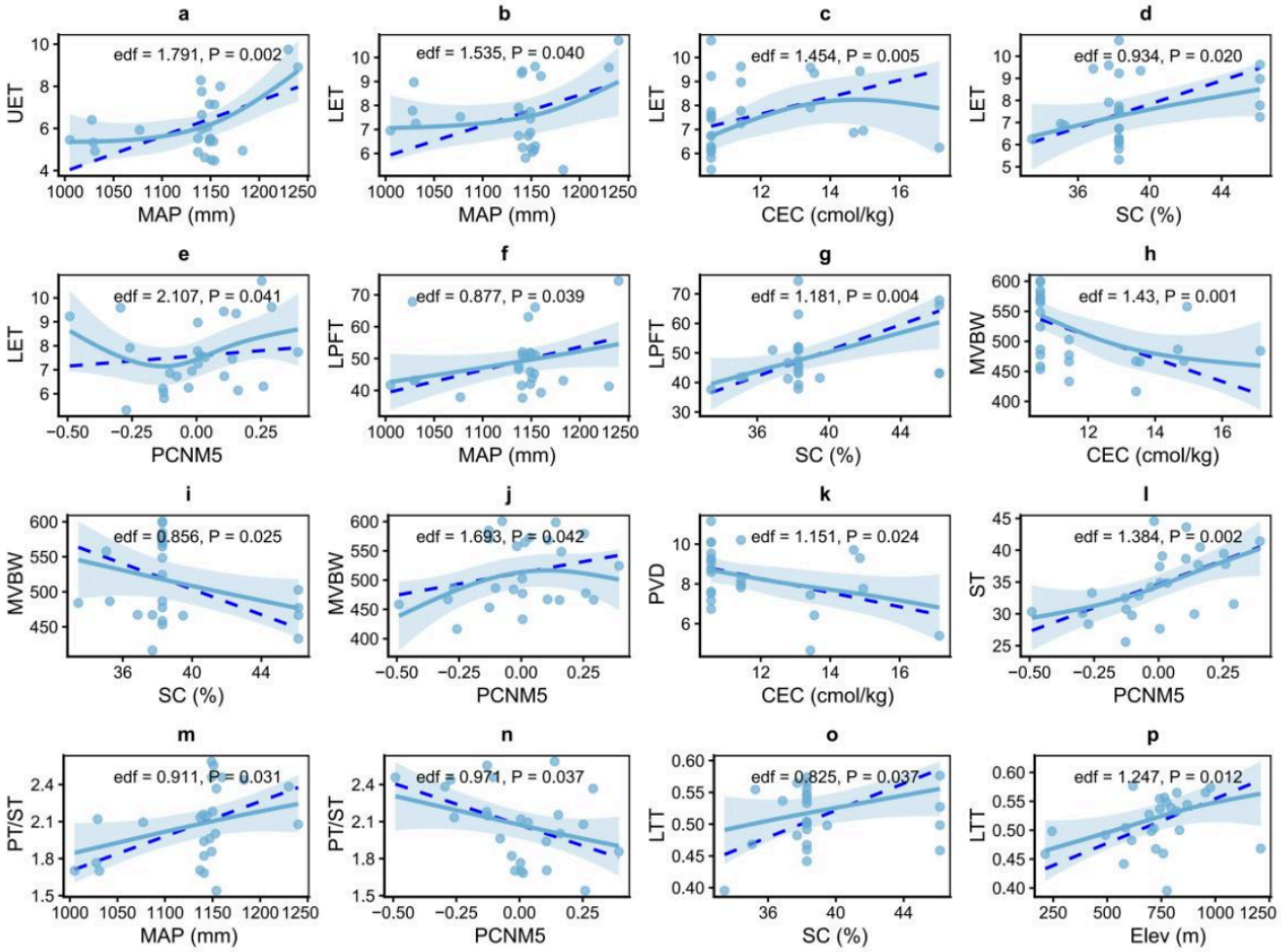

Figure 5

Nonlinear responses of leaf anatomical traits to environmental and spatial drivers. Only significant smooth terms from the GAM ($P < 0.05$) are displayed. The bluelines represent fitted GAM curves; the shaded areas denote the 95% confidence intervals. The blue dashed line represents the fitted line from the linear model (LM). Abbreviations follow those in Fig. 2.

Supplementary Files

This is a list of supplementary files associated with this preprint. Click to download.

- Additionalfile1.docx
- Additionalfile2.docx